

Rice Bran as Source for the Synthesis of Imidazoline-type Inhibitors: Synthesis and Corrosion Performance

E. Reyes-Dorantes^{1,2}, *J. Zúñiga-Díaz*^{1,2}, *A. Quinto-Hernández*¹, *J. Porcayo-Calderon*^{2,3*},
*J.G. Gonzalez-Rodriguez*³, *G.K. Pedraza-Basulto*⁴, *L. Martínez-Gomez*^{2,5}

¹ Tecnológico Nacional de México - Instituto Tecnológico de Zacatepec, Calzada Instituto Tecnológico 27, 62780 Zacatepec, MOR, México

² Instituto de Ciencias Físicas, Universidad Nacional Autónoma de México, Avenida Universidad s/n, 62210 Cuernavaca, MOR, México.

³ CIICAp, Universidad Autónoma del Estado de Morelos, Avenida Universidad 1001, 62209 Cuernavaca, MOR, México.

⁴ Facultad de Ingeniería, UNACAR, C.P. 24180, Ciudad del Carmen, CAM, Mexico.

⁵ Corrosion y Protección (CyP), Buffon 46, 11590 México City, DF, México.

*E-mail: jporcayoc@gmail.com

Received: 7 September 2017 / *Accepted:* 26 October 2017 / *Online Published:* 1 December 2017

Based on its high oil content, this research proposes the use of an agro-industrial by-product (rice bran) as a sustainable option for the synthesis of environmentally friendly corrosion inhibitors. The extraction and characterization of the raw rice bran oil was carried out, and the imidazoline-type inhibitors were synthesized from a 1:3 molar ratio (oil:aminoethylethanolamine). The corrosion inhibitory capacity of the product obtained was evaluated by electrochemical techniques such as potentiodynamic polarization curves and real-time corrosion monitoring. The inhibitory capacity of the synthesized compound was evaluated on an API X-70 steel using a saline solution (3.5% wt. NaCl) saturated with CO₂. The evaluation was performed at three temperatures (30, 50 and 70 °C) and different concentrations of inhibitor (0, 5, 10, 25, 50 and 100 ppm). The results showed that the sustainable use of agro-industrial by-products is a good alternative for the synthesis of environmentally friendly corrosion inhibitors with high inhibition efficiencies.

Keywords: Green inhibitor, Rice Bran, Raw Oil, CO₂ corrosion, Imidazoline.

1. INTRODUCTION

Corrosion is a degradation process of materials that strongly affects the oil industry, of the different processes of degradation that the materials undergo the one caused by the CO₂-dissolved is the one of greater occurrence in the operations of transport of hydrocarbons. In particular, carbon steel

is a very prone material to suffer this type of damage. In the oil industry, carbon steel is the most commonly used material in the construction of pipelines for the transportation of gas and oil. Corrosion problems due to CO₂-dissolved can be solved by using materials with higher corrosion resistance, such as stainless steels however, due to their high costs these materials are rarely used. Therefore, in order to counteract the corrosion problems caused by CO₂-dissolved, it is common to inject corrosion inhibitors in order to extend the useful life of the pipelines. One of the most commonly used corrosion inhibitors for this purpose is the imidazolines-type and its derivatives. It has been shown that these types of compounds possess high inhibition efficiencies and are environmentally friendly [1-7].

Imidazoline-type inhibitors have the characteristic structure of a surfactant molecule formed by a polar head attached to a generally linear hydrophobic tail (typically C16-C18 hydrocarbon chain). It has been proposed that the charged polar group is adsorbed onto metal surface and the hydrocarbon chain extends into the electrolyte [8, 9]. These inhibitors achieve inhibition efficiencies above 95% at doses as low as 10 ppm, and are capable of inhibiting the localized attack of the carbon steel in chlorides-rich electrolytes with CO₂. The high inhibition efficiencies achieved by this type of compound are due to its high affinity with the carbon steel surface to form a molecular film that acts as an effective barrier retarding the corrosion process. The effectiveness of the imidazoline-type compounds depends on its molecular structure, concentration, type of electrolyte as well as the surface characteristics of the alloy (chemical composition and microstructure) [10-12].

The main motivation of this study was to explore the feasibility of the use of unconventional oil sources for the synthesis of environmentally friendly corrosion inhibitors that contribute to the sustainable use of agro-industrial by-products. Therefore, in this study, the synthesis of imidazoline-type corrosion inhibitors from raw rice bran oil was carried out, and its corrosion inhibitory capacity on a API X-70 steel was evaluated in a CO₂-saturated brine (3.5% wt. NaCl). The inhibition efficiency was determined by potentiodynamic polarization curves and real-time corrosion measurements at different temperatures and inhibitor concentration.

2. EXPERIMENTAL PROCEDURE

2.1. Synthesis of Fatty-Imidazolines (2-(2-alkyl-4,5-dihydro-1H-imidazol-1-yl)ethanol Derivatives)

For the synthesis process raw rice bran oil was used. The raw oil was extracted from rice bran collected a few hours after its production from a local mill (Puente de Ixtla, Morelos, MEXICO). The extraction of the raw oil was carried out in a stirred batch system at room temperature, for which a 1:10 ratio, flour to solvent, was used. The chemical and physicochemical characterization of the extracted oil (density, acid index, iodine index, peroxide index, saponification index) was performed according to AOAC methods 920.21, 940.28, 920.158, 965.33 and 920.160, respectively.

The synthesis was performed as described in the literature [13, 14]. In general, the synthesis was performed in two stages. In the first step, 9.2336 g of raw oil with 0.3 moles of aminoethylethanolamine (AEEA) are introduced into the reactor. The mixture is heated to 140 °C with

constant stirring at atmospheric pressure. The course of the reaction is monitored by thin-layer chromatography (TLC), using silica gel as a support, and as eluent a mixture of ethyl acetate and heptane in a ratio of 1:9. The reaction was considered complete until the disappearance of the triglycerides of the oil, this indicates the formation of the corresponding hydroxyethylaminoethylamide of fatty acids (fatty amide) according to the following reaction:

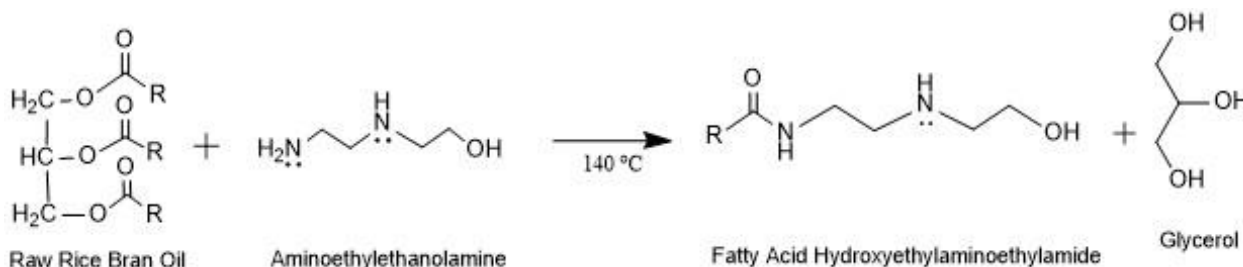


Figure 1. Amidation of raw rice bran oil.

In the second stage of the synthesis process, the reaction product from the previous step is heated to 140 °C, with constant stirring and vacuum (-595 mm Hg). The course of the reaction is followed by thin-layer chromatography (TLC), using silica gel as a support, and as eluent a dichloromethane-methanol mixture in a ratio of 8:2, and 50 μ l of ammonium hydroxide. The reaction was considered complete until the complete disappearance of the fatty amide according to the following reaction:

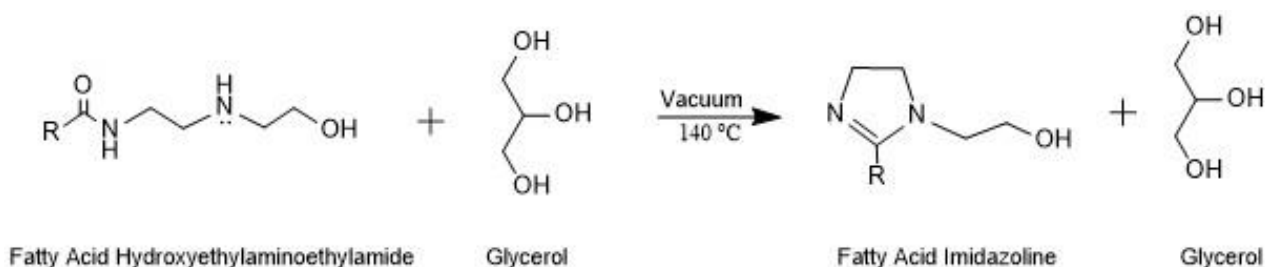


Figure 2. Synthesis of fatty-imidazolines derived from raw rice bran oil.

Both the raw rice bran oil and the reaction products of the synthesis process were characterized by gas chromatography and FTIR analysis.

2.2. Electrochemical Evaluation

The performance of the inhibitor was evaluated as-synthesized, that is, without any further purification process. The electrochemical techniques used were potentiodynamic polarization and corrosion measurements in real time. For the potentiodynamic polarization tests, a three electrode electrochemical cell was used, with a Pt wire as the reference electrode and a graphite rod as the

counter electrode. The tests were performed on an ACM Instruments zero-resistance ammeter (ZRA) coupled to a personal computer. The working electrode (WE) consisted of an API X-70 steel sample with a reaction area of 1 cm^2 encapsulated in acrylic resin. The WE was abraded with SiC abrasive paper to grade 600, washed with ethyl alcohol and distilled water, dried with dry air and immediately used in the tests. A solution of NaCl (3.5% by weight) saturated with CO_2 was used as the corrosive medium. The brine was bubbled with CO_2 two hours before the start of the test, and the bubbling was maintained throughout the test. The tests were performed at 30, 50 and 70 °C with gentle agitation. The inhibitor (fatty-imidazolines) was dissolved in pure 2-propanol (5% w/w), and its performance was evaluated at 0, 5, 10, 25, 50 and 100 ppm. Prior to the potentiodynamic polarization the working electrode was allowed to stabilize into electrolyte for 24 hours. This condition was chosen in order that the inhibitor reaches the maximum surface coverage of the working electrode. Potentiodynamic polarization was performed from -400 mV to 600 mV with respect to E_{corr} value at a scanning rate of 1 mV/s. From the polarization curves the electrochemical parameters (corrosion potential, corrosion current density, and Tafel slopes) were obtained.

An arrangement of three identical electrodes was used for the real-time corrosion measurements. The probe was formed by three samples (0.3 x 1.0 x 1.0 cm) of API X-70 steel, and a conductive Ni20Cr wire was welded on one side of each steel sample. The arrangement of three electrodes was encapsulated in acrylic resin, abraded with abrasive paper to grade 600, washed with ethyl alcohol and distilled water, dried and immediately employed in the electrochemical tests. Real-time measurements were performed with a SmartCET equipment based on a combination of electrochemical techniques such as electrochemical noise (EN), polarization resistance (PR) and harmonic distortion analysis (HDA), and as a result of this interrelationship the corrosion rate (mpy) of the API X-70 steel is obtained. In short, each measurement cycle is 430 seconds, in the first 300 seconds the EN (in current and potential) is measured, after that, both PR and HDA measurements are made for 100 seconds, and finally, the electrolyte resistance is measured for 30 seconds. In the PR measurement a small disturbance ($\pm 25 \text{ mV}$) to the potential is applied across the electrodes, and the current response is measured. From the slope of the potential-current sweep the polarization resistance is obtained, which is inversely proportional to the corrosion current density. With the polarization resistance value obtained and with fixed values of the Tafel slopes (B_a , B_c), it is possible to calculate the corrosion current density (I_{corr}) from the Stern-Geary equation. HDA is essentially a low frequency impedance measurement technique where the response of the current to a low frequency voltage sine wave is distorted due to the non-linearities of the charge transfer process. The HDA technique applies a voltage perturbation at frequencies of 10, 20 and 30 mHz with an amplitude of 50 mV peak-to-peak and analyzes the current response for each applied frequency. By means of this technique it is possible to obtain the kinetic parameters of the corrosion process using instantaneous values of the Tafel slopes, that is to say, no presumed or estimated values are used. The analysis between the low frequency impedance and the applied voltage is analyzed in order to determine the actual values of the Tafel slopes (B_a , B_c) which are used to calculate the corrosion current density (I_{corr}) from the Stern-Geary equation.

In both cases, the corrosion rate is calculated from the following relationship:

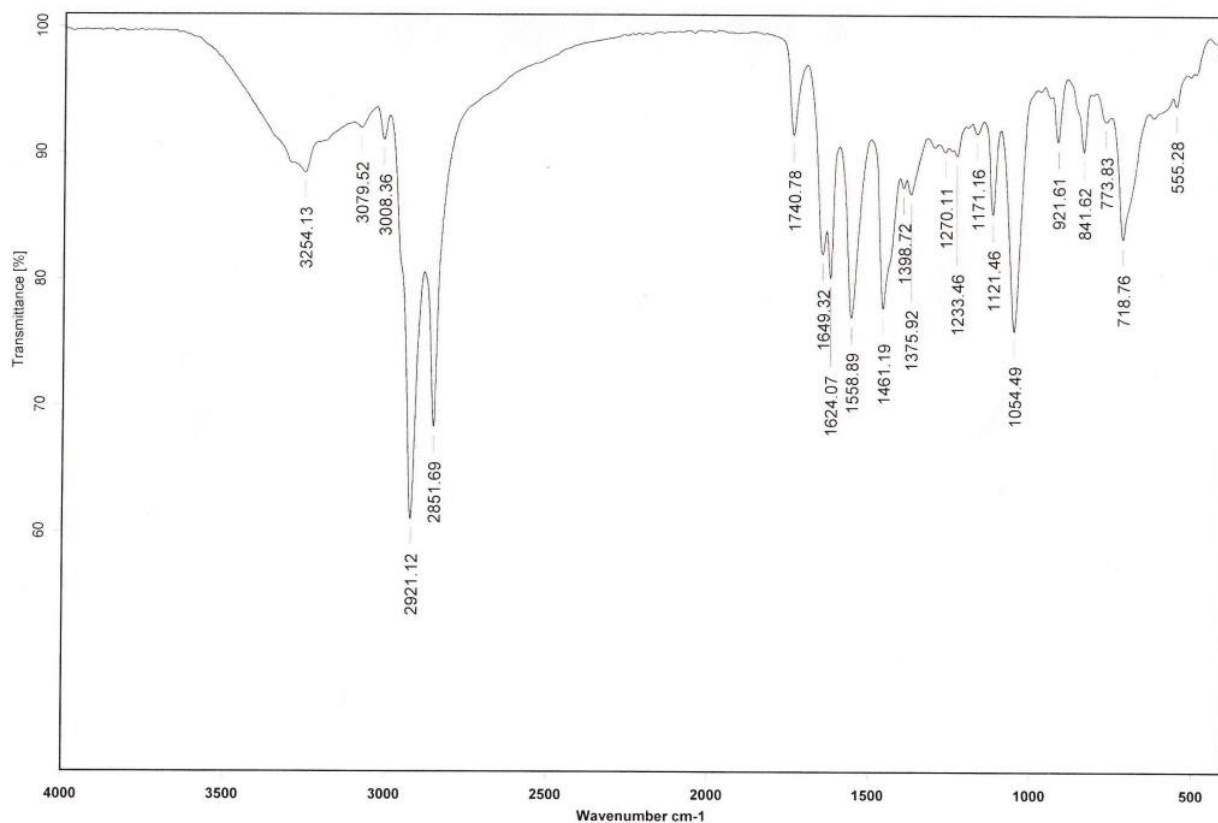
$$CR (mpy) = \frac{0.1288 i_{corr} W}{\rho n}$$

Where, CR is the corrosion rate, i_{corr} is the corrosion current density ($\mu A/cm^2$), W is the atomic weight of the oxidized element, and n is the valence of the oxidized element. The details of this real-time monitoring technique are described elsewhere [15, 16].

3. RESULTS AND DISCUSSION

3.1. Synthesis of the Inhibitor

The raw oil content of rice bran was 21%, and its chemical composition indicated a content of 48.48% oleic acid, 35.26% linoleic acid and 14.54% palmitic acid (wt. %). Values similar to those reported for this type of oil [17].



(a)

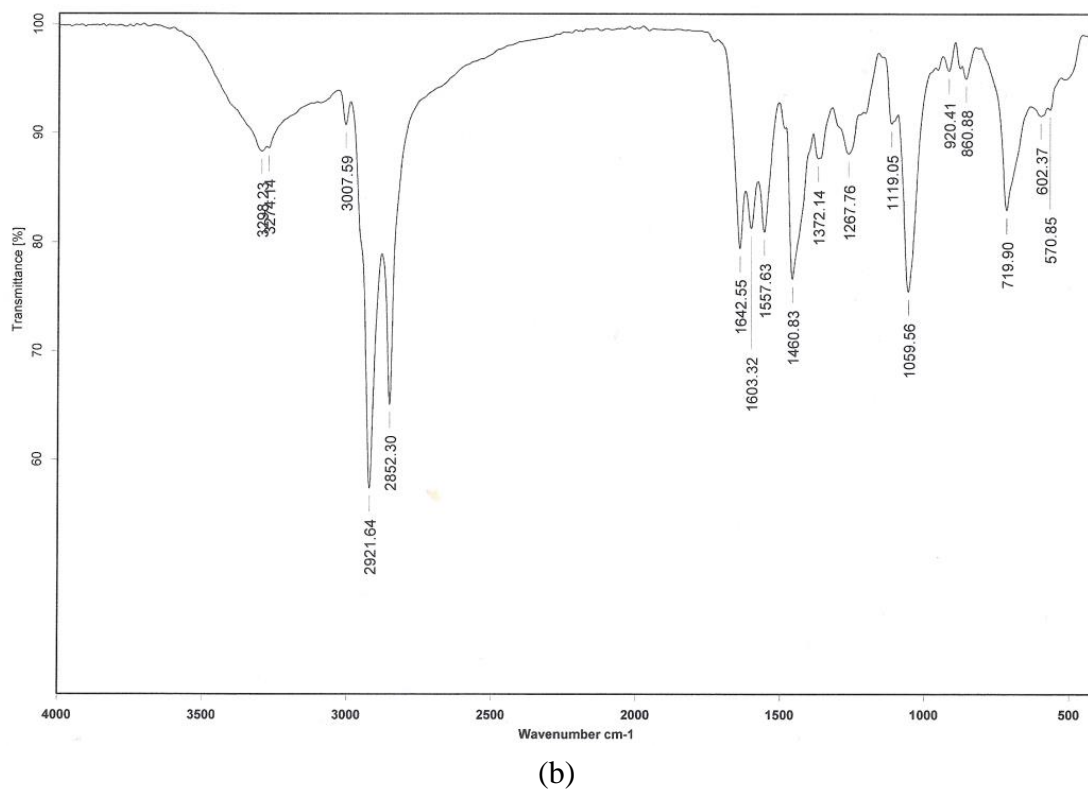


Figure 3. FT-IR spectra of imidazoline-type inhibitor synthesis from raw rice bran oil, (a) initial mixture (raw oil-aminoethylethanolamine), (b) reaction products (Fatty imidazoline).

Figure 3 shows the FT-IR spectra of the reaction mixture and the reaction products of the imidazoline-type inhibitor synthesis process. In the reaction mixture at 1740 cm^{-1} , the band corresponding to the C=O stretch of the oil triglycerides disappears (Figure 3a), and a band appears at 1640 cm^{-1} (Figure 3b), the presence of this signal is characteristic of the peaks corresponding to amidation products [13, 14]. The band corresponding to the -N-H stretch of the secondary amide appears at 3299 cm^{-1} , and at 1603 cm^{-1} the band corresponding to the C=N bond is observed, its presence indicating the formation of the imidazoline ring due to the cyclization process [13, 18]. Other studies report that the presence of the double bond of the imidazoline group can be observed in the range of 1600 cm^{-1} to 1665 cm^{-1} depending on the substituent groups attached in the C2 and N1 of the imidazolinic ring [8].

Based on the chemical composition of the raw oil, it is assumed that the molecular structure of the synthesized imidazolines is as shown in Figure 4, and in the proportion suggested according to the fatty acid content of the raw oil. Structural calculations show that independently of the groups attached to the imidazoline ring both the bond lengths of the structures as the internal bond angles of the imidazolinic ring are not appreciably affected and also indicate that the region richest in electrons available for donation is in the area between N1 and N2 [8]. The structural rigidity of the imidazoline ring suggests that it possesses a nearly planar configuration, and that its high electron density favors the imidazoline ring being preferentially adsorbed by a flat-adsorption process, and the alkyl chain is projected into the electrolyte [4, 7, 19-20].

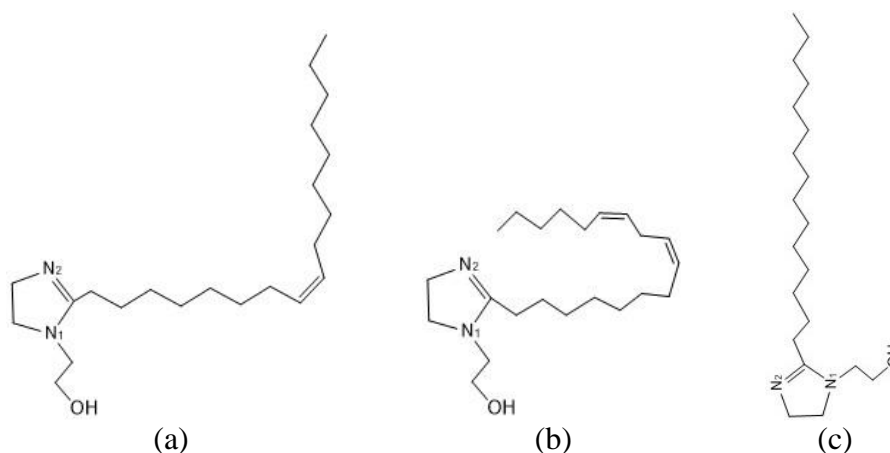


Figure 4. Fatty-Imidazoline derivatives from de raw rice bran oil, a) oleic hydroxyethyl-imidazoline, b) linoleic hydroxyethyl-imidazoline, c) palmitic hydroxyethyl-imidazoline.

3.2. Potentiodynamic Polarization

Figures 5 to 7 show the polarization curves for API X-70 steel in CO_2 -saturated brine, and different concentrations of inhibitor at 30, 50 and 70 °C, respectively. The polarization curves correspond to the WE polarization after 24 hours of stabilization in the electrolyte as established in the experimental procedure. It is observed that in the absence of inhibitor at 30 and 50 °C, the tendency of the anodic branch indicates that the steel is undergoing a continuous dissolution process. At 70 °C a tendency to passivation is observed possibly due to the presence of a protective layer based on FeCO_3 , however the protection is limited since to more anodic potentials an active behavior is again observed. This may be due to the presence of imperfections (porosity and cracks) by which the electrolyte penetrated and caused the detachment of the protective layer [21]. However, in the presence of the inhibitor, in all cases it is observed that the polarization curves are located in the region of lower current density due to a decrease in the rate of corrosion of the steel. In the anodic branch it is possible to observe a greater slope in the region close to the corrosion potential, this increase in the anodic slope is related to a decrease in the active behavior of the steel due to the formation of an inhibitor film on its surface. At 30 °C and 50 °C the highest increase in the anodic slope is observed at concentrations of 5 and 10 ppm respectively, and at 70 °C occurs at concentrations above 10 ppm. It is interesting to note that the change of the anodic slope to a more active behavior (possibly due to the detachment of the inhibitor film), is observed around 150, 200 and 250 mV above E_{corr} at 30, 50 and 70 °C respectively, for the inhibitor concentrations indicated. This may suggest that increasing the temperature favors the formation of an inhibitory film with greater protection capacity. The behavior of the anodic branch suggests that the addition of the inhibitor suppressed the dissolution reactions of Fe [1, 22-24].

The cathode branch is similar to all test temperatures, this because the reduction reaction is the same. In the absence of inhibitor it is observed that by increasing the test temperature the cathodic branch is displaced at higher current densities. This is normal for thermally activated processes, since the reaction rate is enhanced by increasing the temperature. However, in the presence of the inhibitor the cathodic branches are shifted to lower current densities depending on the concentration of added

inhibitor. The largest displacement is observed with 5 ppm, 10 ppm and 25 ppm at 30, 50 and 70 °C, respectively. This shift suggests that the presence of the inhibitor may be interfering with the reduction reaction.

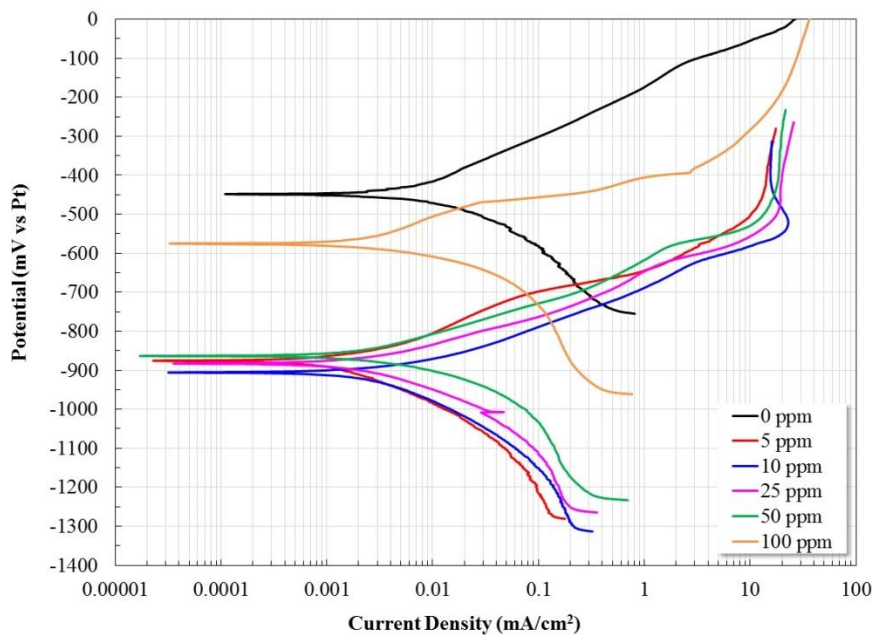


Figure 5. Potentiodynamic polarization curves for API X-70 steel in CO₂-saturated brine at different concentrations of the fatty-imidazolines at 30 °C (after 24 hours of stabilization).

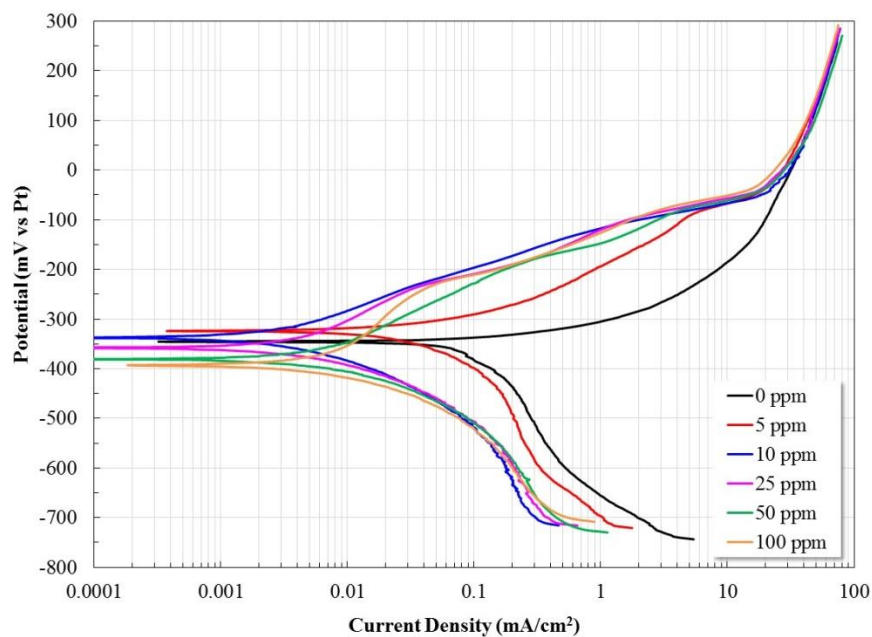


Figure 6. Potentiodynamic polarization curves for API X-70 steel in CO₂-saturated brine at different concentrations of the fatty-imidazolines at 50 °C (after 24 hours of stabilization).

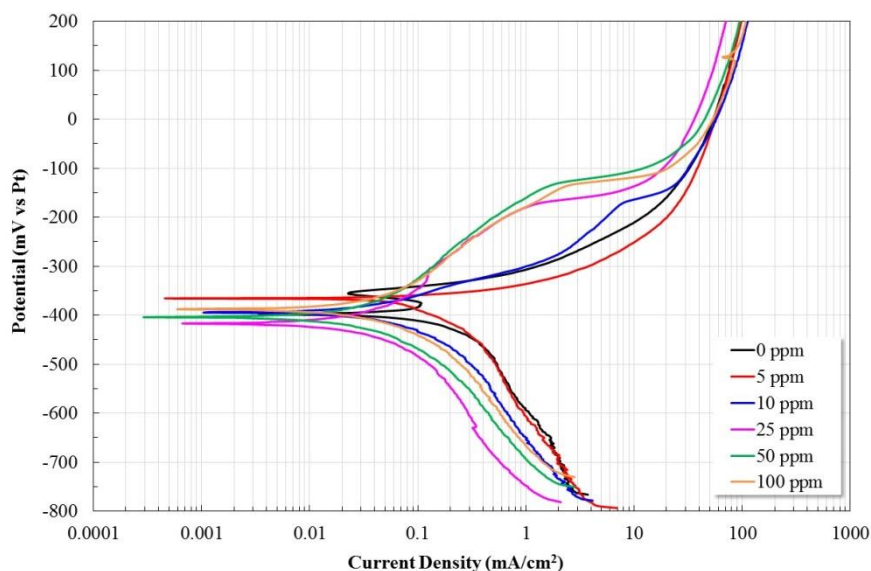


Figure 7. Potentiodynamic polarization curves for API X-70 steel in CO₂-saturated brine at different concentrations of the fatty-imidazolines at 70 °C (after 24 hours of stabilization).

It is known that the CO₂ saturation of a saline solution will cause a decrease in the pH of the solution due to the formation of carbonic acid ($\text{CO}_2 + \text{H}_2\text{O} = \text{H}_2\text{CO}_3$), reaching a balance between the hydrogen ions (H^+) and the CO₂ dissolved [25]. Under these conditions, the suggested reduction reactions can be H^+ reduction, H_2CO_3 dissociation and H_2O reduction [23-24, 26]. Because the imidazoline derivatives are strong bases [27], then the observed displacement of the cathodic branches can be due to the neutralization of hydrogen ions (H^+), or because the reduction of the CO₂ solubility limit in the solution.

However, it has also been observed that the addition of similar inhibitors only slightly modifies the pH of the solution [28].

Tables 1 to 3 show the variation of the electrochemical parameters obtained from Figures 5 to 7. Particularly at 50 and 70 °C the trend of the values show the same behavior, the observed discrepancies at 30 °C may be due to a decrease in the solubility and dispersion of the inhibitor in the electrolyte. Regarding E_{corr} values at 50 and 70 °C, nobler E_{corr} values are observed at concentrations up to 10 ppm, and at higher concentrations slightly more active E_{corr} values, but with a tendency to converge at high concentrations regardless of temperature, however, at 30 °C the E_{corr} values are more active at all concentrations but with a tendency toward noble values as the inhibitor concentration increases. The trend of the anodic slope values show an increase with the concentration of inhibitor and temperature, only at 30 °C a decrease is observed at low concentrations (5 ppm) but at higher concentrations its values tend to increase. The constant increase in the anodic slope suggests the formation of a passive film, where this passive film is formed by the inhibitor molecules adsorbed onto steel surface. On the other hand, the general behavior of the cathodic slope values shows lower values than that observed in the absence of inhibitor and increase with the test temperature. The above is consistent with what has previously been described with respect to a reduction in the current density of the cathodic branch by increasing the concentration of inhibitor. The trend of the I_{corr} values clearly

shows a decrease in the corrosion rate of the steel due to the addition of the inhibitor however, its effect is more noticeable at low concentrations (≤ 25 ppm).

Table 1. Electrochemical parameters as a function of the inhibitor concentration at 30 °C.

Inhibitor concentration [ppm]	E _{corr} [mV]	B _a [mV/Dec]	B _c [mV/Dec]	I _{corr} [mA/cm ²]
0	-449	133	104	0.01978
5	-876	107.4	159	0.00202
10	-906	76.1	154.1	0.00235
25	-883	74.7	105.4	0.00279
50	-864	90	100	0.00304
100	-576	117.2	65.2	0.00281

Table 2. Electrochemical parameters as a function of the inhibitor concentration at 50 °C.

Inhibitor concentration [ppm]	E _{corr} [mV]	B _a [mV/Dec]	B _c [mV/Dec]	I _{corr} [mA/cm ²]
0	-346	42.5	308.3	0.0864
5	-324	100	280	0.0399
10	-338	119	190	0.00405
25	-358	164	120	0.00964
50	-381	214	141	0.011
100	-393	291.2	143	0.0144

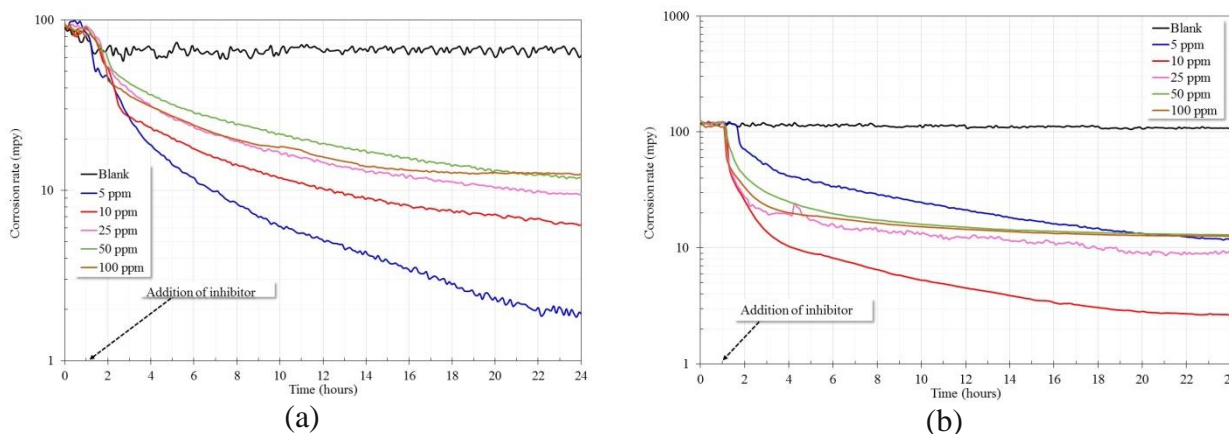
The maximum reduction of the corrosion rate is observed at 5, 10 and 25 ppm at 30, 50 and 70 °C, respectively. At concentrations of inhibitor below those concentrations, the inhibitor is not able to achieve a surface coverage that prevents the diffusion of the electrolyte, i.e., the presence of unprotected sites prevails, however, at higher concentrations electrostatic repulsion forces can be generated between the adsorbed molecules causing their desorption and the presence of unprotected sites. This agrees perfectly with the concentrations that caused the greater displacement of the cathodic branches to the region of lower current density. Previous evidence suggests that the inhibitor evaluated acts as an inhibitor of the mixed type.

Table 3. Electrochemical parameters as a function of the inhibitor concentration at 70 °C.

Inhibitor concentration [ppm]	E _{corr} [mV]	B _a [mV/Dec]	B _c [mV/Dec]	I _{corr} [mA/cm ²]
0	-397.4	31.28	371.6	0.2
5	-365.6	67.13	335.7	0.125
10	-394	105.4	320.1	0.09
25	-407	175.9	302.8	0.0508
50	-404	228.2	196.5	0.0679
100	-388	299.9	248	0.0786

3.3. Real-time Corrosion Monitoring

Figure 8 shows the effect of the addition of the inhibitor on corrosion rate, based on PR measurements of the API X-70 steel exposed to CO₂-saturated brine at different temperatures. In all cases, the inhibitor was added 60 minutes after the measurements were initiated. In the absence of inhibitor it is observed that the corrosion rate of the steel is always higher regardless of the test temperature. At 70 °C a tendency to decrease as a function of time is observed, this behavior is associated to the formation of a protective layer due to the precipitation of FeCO₃ onto steel surface, however, at lower temperatures this phenomenon is not evident because the FeCO₃ precipitation is favored at temperatures greater than 50 °C or greater reaction times. However, in the presence of the inhibitor it is observed that the steel corrosion rate decreases notably but depending on the inhibitor concentration. In all cases a drastic fall in the corrosion rate values is observed in the first 3-4 hours after the inhibitor has been added, and subsequently the corrosion rate tends to decrease slowly without reaching a steady state during the test. This tendency suggests that the inhibitor possesses a high affinity towards the metallic surface, being able to form a protective film between the steel surface and the electrolyte, thus limiting the access of the aggressive species. The optimum concentration of inhibition increases with temperature, being 5, 10 and 25 ppm at 30, 50 and 70 °C, respectively. Higher or lower concentrations than those indicated, do not reduce the rate of corrosion to the levels of the optimum concentrations. Generally, this is because at low concentrations the inhibitor molecules are not sufficient to achieve the desired surface coverage, and on the other hand, at higher concentrations, the amount of inhibitor molecules is excessive such that repulsion forces are created between the functional groups (imidazoline ring, double bonds of the hydrocarbon chains, etc.), these repulsive forces prevent the inhibitor molecules from easily reaching the metal surface [6], or when the adsorbed molecules exceed a certain number can be generated electrostatic repulsion forces between them causing their desorption and the occurrence of unprotected areas [29], or due to the change in orientation of the adsorbed molecules [30, 31]. Regardless of the temperature the inhibitor decreased the steel corrosion rate by up to two orders of magnitude.



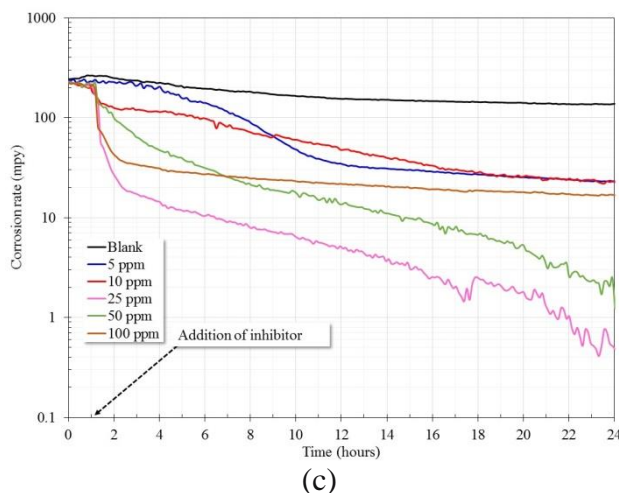


Figure 8. Variation of corrosion rate determined by PR (real-time monitoring) versus time for API X70 steel exposed to a CO₂-saturated brine with different concentrations of inhibitor, a) 30 °C, b) 50 °C, c) 70 °C.

Based on the data of Figure 8, the variation in the inhibition efficiency as a function of time was calculated (Figure 9). The inhibition efficiency was determined according to the following relationship:

$$E(\%) = \frac{CR_i - CR_b}{CR_i} * 100$$

Where CR_b is the corrosion rate in absence of inhibitor, and CR_i is the corrosion rate in presence of inhibitor. It can be seen that for the optimum inhibitor concentration, its inhibition efficiency was at least 98% at all test temperatures. However, in the test period evaluated, steady state was not reached, whereby the inhibition efficacy may increase to longer test times. According to the results observed in Figure 9, the maximum inhibition efficiency was obtained with 5, 10 and 25 ppm at 30, 50 and 70 °C respectively. It is observed that increasing the test temperature increases the amount of inhibitor required to achieve maximum inhibition efficiency. That is to say, by increasing the test temperature, the corrosion rate is increased and therefore a greater amount of inhibitor is required to counteract it. With inhibitor amounts greater or lower than those indicated, maximum inhibition efficiency is not obtained. This is because at lower concentrations the amount of inhibitor molecules is insufficient to achieve maximum surface coverage, and at higher concentrations the occurrence of electrostatic repulsive forces is possible which prevent efficient packaging of the inhibitor molecules onto metal surface.

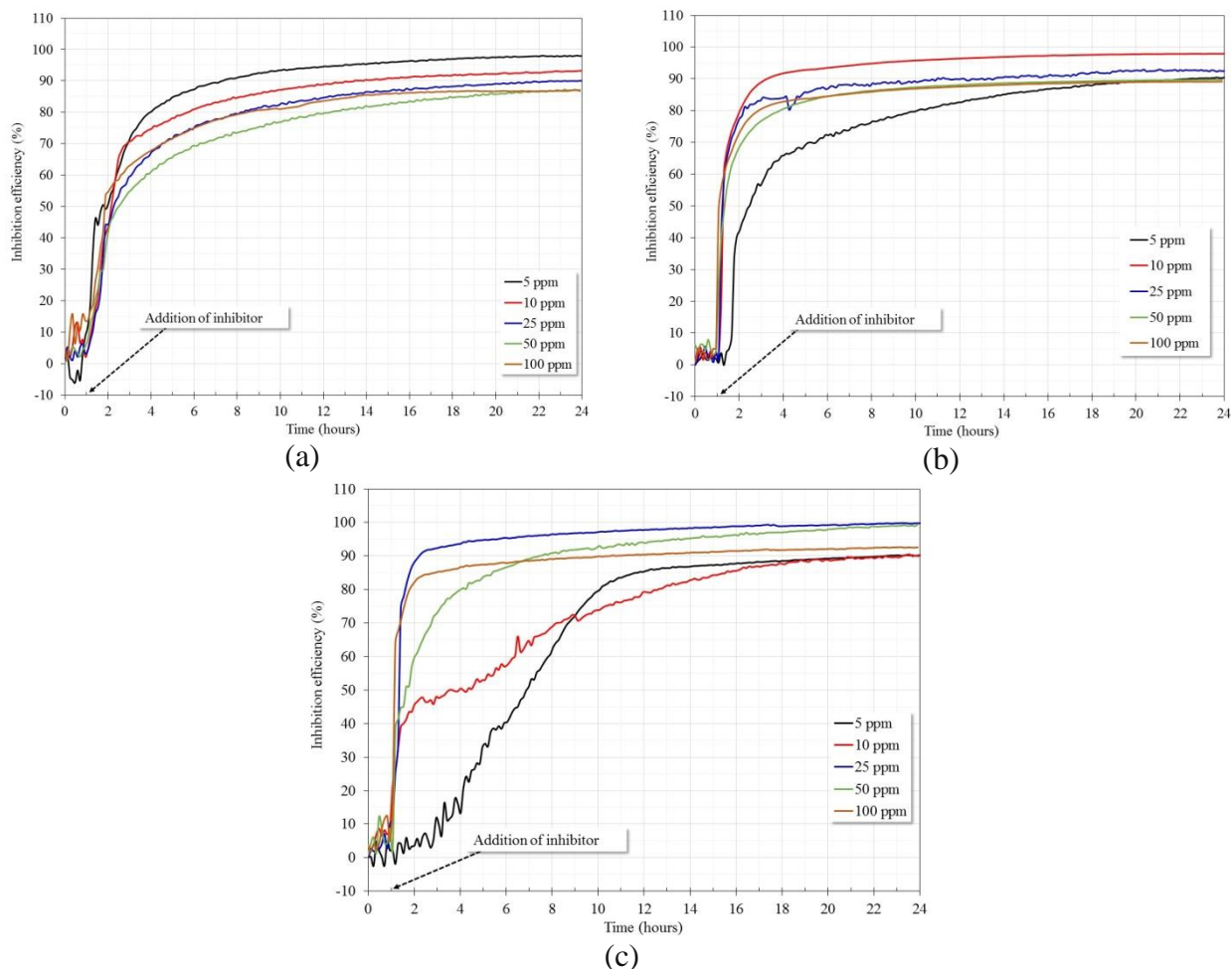


Figure 9. Variation of inhibition efficiency determined from PR measurements (real-time monitoring) in CO₂-saturated brine, a) 30 °C, b) 50 °C, c) 70 °C.

Figure 10 shows the effect of the inhibitor addition on the corrosion rate determined from HDA as a function of time for API X-70 steel exposed in CO₂-saturated brine at 30, 50 and 70 °C. This technique is based on the perturbation of an AC signal and the analysis of the nonlinear response in the frequency domain [15, 16]. Corrosion rates are similar to those obtained from PR measurements (Figure 8). However, in the presence of the inhibitor disturbances are observed in the measurements, in general these transients have been associated with adsorption-desorption processes of the inhibitor molecules [5]. HDA-based corrosion rate measurements employ dynamic Tafel slopes instead of fixed values, for this reason in the PR-based corrosion rate measurements these disturbances are not observed.

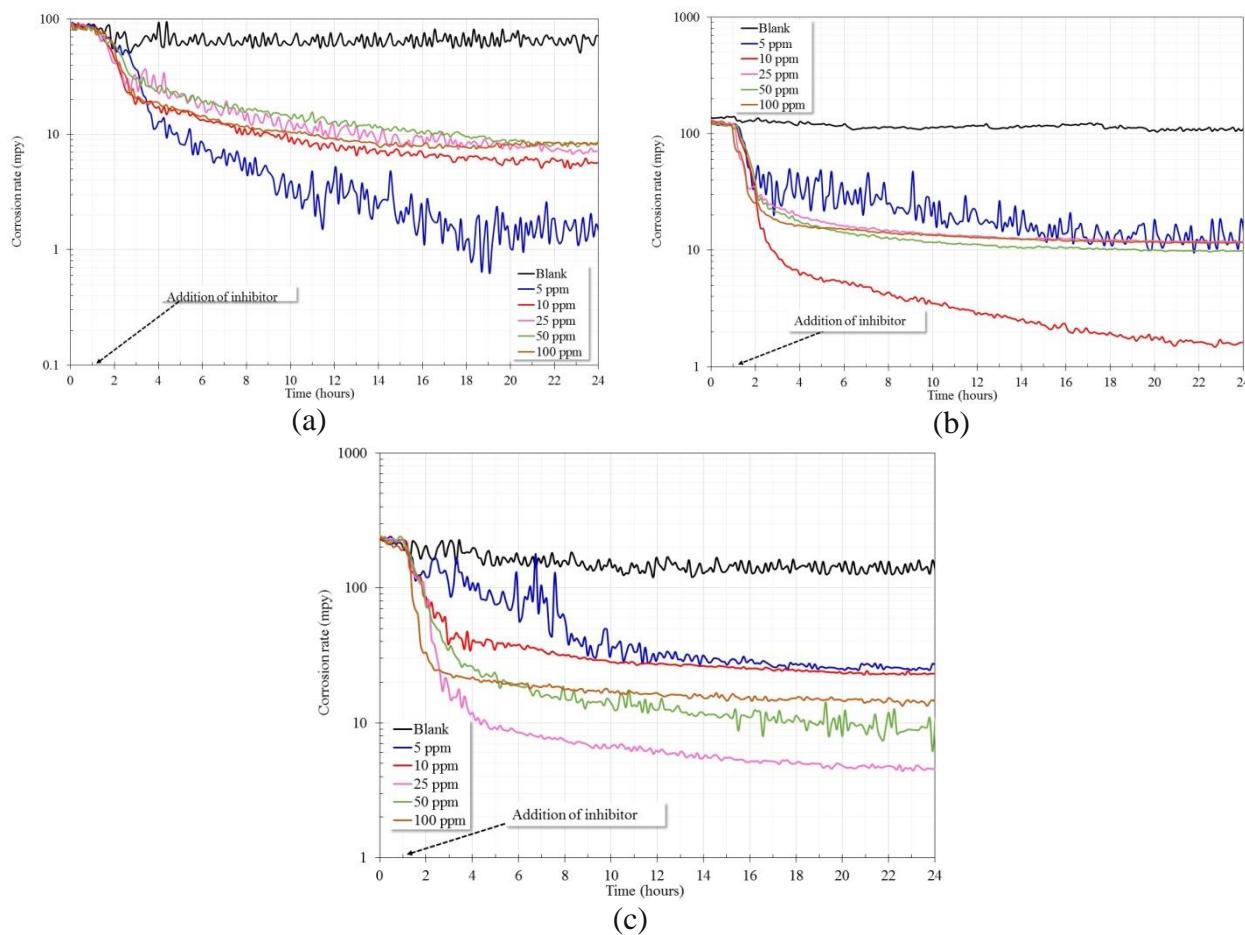
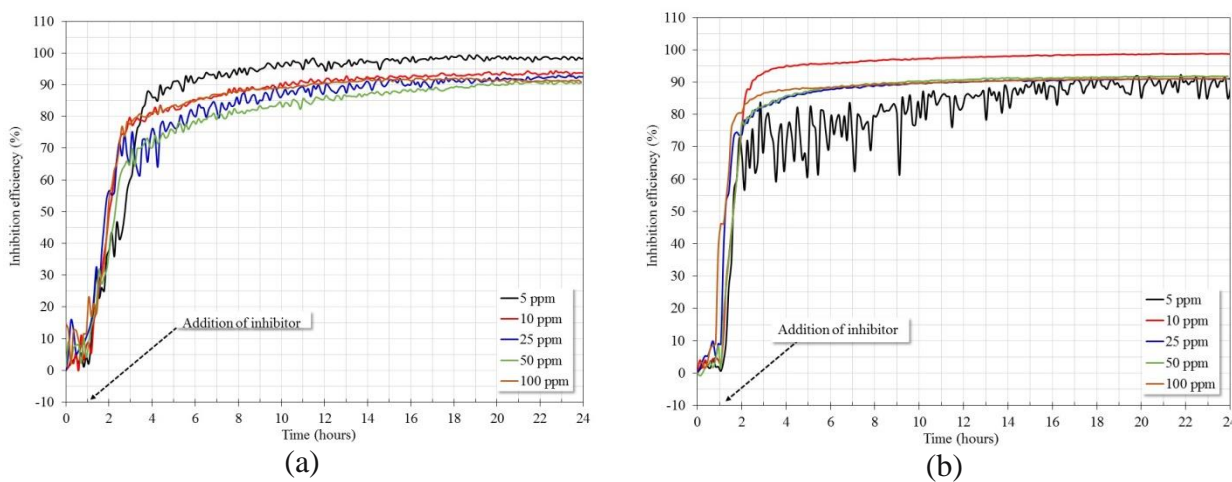


Figure 10. Variation of corrosion rate determined by HDA (real-time monitoring) versus time for API X70 steel exposed to a CO₂-saturated brine with different concentrations of inhibitor, a) 30 °C, b) 50 °C, c) 70 °C.

Figure 11 shows the change in the inhibition efficiency from the corrosion rate measurements derived from the HDA measurements (Figure 10). The results are similar to those calculated from the PR measurements (Figure 9), inhibition efficiencies of at least 98% are observed for optimal concentrations with a tendency to increase steadily.



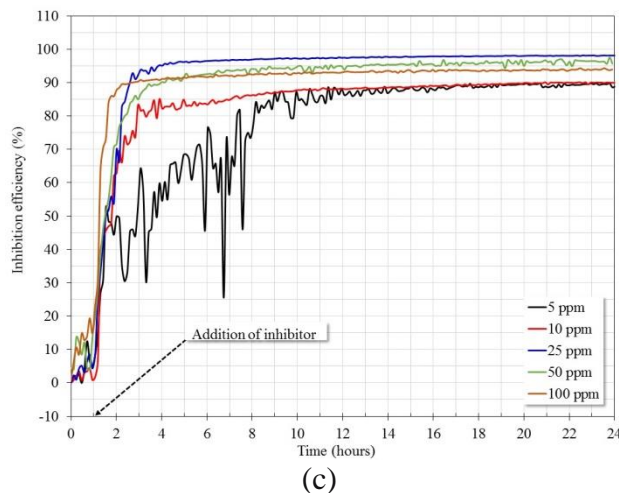


Figure 11. Variation of the inhibition efficiency determined from HDA measurements (real-time monitoring) in CO₂-saturated brine, a) 30 °C, b) 50 °C, c) 70 °C.

Again, the high inhibition efficiency of the synthesized inhibitor is corroborated. Inhibition efficiency curves show instabilities due to the adsorption-desorption processes mentioned above. Again it is observed that the maximum inhibition efficiency is achieved at concentrations of 5, 10 and 25 ppm at 30, 50 and 70 °C.

3.4. Adsorption Isotherms

In order to determine the type of interaction (physisorption, chemisorption) between the inhibitor and steel surface, the adsorption isotherms were calculated based on the PR measurements. During the adsorption process the displacement and substitution of the water molecules by the inhibitor molecules is carried out and the type of interaction can be determined from the corrosion rate measurements. The experimental data were adapted to the Langmuir adsorption model according to the following equation:

$$\frac{C_i}{\theta} = \frac{1}{K_{ads}} + C_i$$

Where C_i is the concentration of inhibitor (mol/l), K_{ads} is the adsorption equilibrium constant, and θ is the surface coverage of the inhibitor. The surface coverage of the inhibitor (θ) is determined according to:

$$\theta = 1 - \frac{CR_u}{CR_i}$$

In this relationship CR_u is the corrosion rate in the absence of inhibitor, and CR_i is the corrosion rate in the presence of inhibitor. For the calculations, the CR_i values employed corresponded

to the average of the last four hours of the corrosion rate measurements reported in Figure 8. Figure 12 shows the adsorption isotherms determined at the three test temperatures. The correlation of the experimental data to the model used indicates that the adsorption process of the inhibitor molecules follows the Langmuir adsorption model.

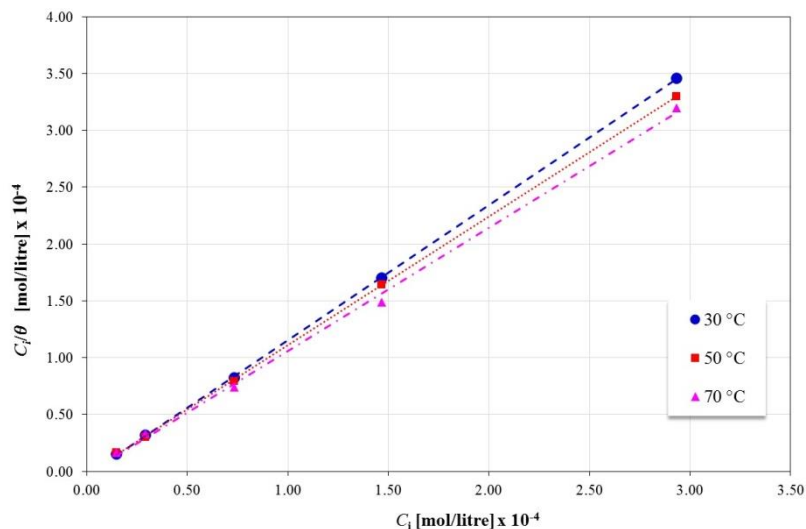


Figure 12. Langmuir adsorption isotherms for the fatty-imidazolines tested in CO₂-saturated brine at different temperatures.

The correlation of the experimental data showed values of the adsorption equilibrium constant, K_{ads} , of 29.41×10^4 , 46.08×10^4 , 38.16×10^4 , for 30, 50 y 70 °C respectively. The magnitude of the K_{ads} values are indicative of the high adsorption capacity of the inhibitor evaluated and its high inhibition efficiency as already described. Based on the K_{ads} values, the standard free energy of adsorption at each temperature was determined according to:

$$K_{ads} = \frac{1}{55.5} e^{\left(\frac{-\Delta G_{ads}^0}{RT}\right)}$$

In this relationship G_{ads}^0 (J mol⁻¹) is the standard free adsorption energy, R is the gas constant (8.314472 J/K-mol), T (K) is the absolute temperature and 55.5 corresponds to the concentration of Water in the solution. The calculation of G_{ads}^0 allows determinate the mode of adsorption of the inhibitor molecule, either adsorption by physisorption or by chemisorption. Usually values less than -20 kJ mol⁻¹ are indicative of a physisorption process, and values above -40 kJ mol⁻¹ are characteristic of a chemisorption process. In the adsorption processes by chemisorption, coordinate bonds are formed between the inhibitor molecule and the metal surface. The calculated ΔG_{ads}^0 values were -41.88, -45.85 and -48.15 kJ mol⁻¹ for 30, 50 and 70 °C, respectively. The magnitude of these values indicates that between the inhibitor molecule and the metal surface a spontaneous adsorption process occurs by chemisorption, possibly due to the interaction between the iron atoms (*d* orbital) and the N atoms of the imidazoline ring.

The above results demonstrate that the imidazoline-type compounds derived from raw rice bran oil act as excellent corrosion inhibitors. In this case, the imidazolinic ring promotes the adsorption by chemisorption of the molecule to the metal surface, while the hydrocarbon tail is projected towards the solution forming a protective monolayer [32]. In addition, when the hydrocarbon chains have double bonds (as in this case) the adsorption process is enhanced, as well as the inhibition efficiency [5, 7, 33].

4. CONCLUSIONS

Rice bran is an agro-industrial by-product with a high oil content which can be used for the synthesis of corrosion inhibitors. The electrochemical performance of the synthesized inhibitor shows high protection efficiencies. Evaluations performed through potentiodynamic polarization curves showed that the anodic branch shifts at lower current densities, the anodic slope increases, and the corrosion current density decreases. These changes are associated with an increase in the activation energy of the Fe dissolution process due to adsorption of the inhibitor onto metal surface. Real-time corrosion rate measurements confirmed that the inhibitory capacity is a function of both inhibitor concentration and temperature, being 5, 10 and 25 ppm the optimum concentrations at 30, 50 and 70 °C, respectively, and the inhibition efficiencies were at least 98%. Calculations of the standard free adsorption energy indicated that between the inhibitor molecule and the metal surface occur a spontaneous adsorption process by chemisorption. According to the molecular structure of the inhibitor it can be said that the imidazolinic ring promotes the adsorption by chemisorption and the hydrocarbon tail is projected towards the solution forming a protective monolayer, in addition the presence of the double bonds of the hydrocarbon tails enhance the adsorption process.

ACKNOWLEDGEMENTS

Financial support from Consejo Nacional de Ciencia y Tecnología (CONACYT, México) (Project 198687) is gratefully acknowledged. E. Reyes-Dorantes and J. Zúñiga-Díaz thank the CONACYT (Mexico) for the financial support given to realize their postgraduate studies

CONFLICT OF INTERESTS

The authors declare that there is no conflict of interests regarding the publication of this paper.

References

1. G. Zhang, C. Chen, M. Lu, C. Chai and Y. Wu, *Mater. Chem. Phys.*, 105 (2007) 331.
2. P.C. Okafor, X. Liu and Y.G. Zheng, *Corros. Sci.*, 51 (2009) 761.
3. J. Liu, W. Yu, J. Zhang, S. Hu, L. You and G. Qiao, *Appl. Surf. Sci.*, 256 (2010) 4729.
4. J. Zhang, G. Qiao, S. Hu, Y. Yan, Z. Ren and L. Yu, *Corros. Sci.*, 53 (2011) 147.
5. J. Porcayo-Calderon, I. Regla, E. Vazquez-Velez, L.M. Martínez de la Escalera, J. Canto and M. Casales-Díaz, *J. Spectrosc.*, 2015 (2015) 1.
6. J. Porcayo-Calderon, L. M. Martínez de la Escalera, J. Canto and M. Casales-Díaz, *Int. J. Electrochem. Sci.*, 10 (2015) 3160.

7. S. Godavarthi, J. Porcayo-Calderon, M. Casales-Diaz, E. Vazquez-Velez, A. Neri and L. Martinez-Gomez, *Curr. Anal. Chem.*, 12 (2016) 476.
8. J. Cruz, L.M.R. Martinez-Aguilera, R. Salcedo and M. Castro, *Int. J. Quantum Chem.*, 85 (2001) 546.
9. W. Durnie, R. De Marco, A. Jefferson and B. Kinsella, *J. Electrochem. Soc.*, 146 (1999) 1751.
10. M.P. Desimone, G. Gordillo and S.N. Simison, *Corros. Sci.*, 53 (2011) 4033.
11. D.A. Lopez, S.N. Simison and S.R. de Sanchez, *Corros. Sci.*, 47 (2005) 735.
12. P.C. Okafor, C.B. Liu, Y.J. Zhu and Y.G. Zheng, *Ind. Eng. Chem. Res.*, 50 (2011) 7273.
13. S. Yoo, Y. Kim, K. Chung, S. Baik and J. Kim, *Corros. Sci.*, 59 (2012) 42.
14. D. Kumar, S.M. Kim and A. Ali, *New J. Chem.*, 39 (2015) 7097.
15. R.D. Kane and S. Campbell, *CORROSION/2004*, Paper No. 04579. Houston, TX: NACE International, p. 15.
16. D.C. Eden, D.A. Eden, I.G. Winning and D. Fell, *CORROSION/2006*, Paper No. 06321, Houston, TX: NACE International, p. 15.
17. A.G.G. Krishna, P.A. Prashantha, A. Pragasam, K.V. Raghavendra and S. Matoon, *J. Food Lipids*, 10 (2003) 329.
18. I.A. Aiad, A.A. Hafiz and A.O. Habib, *J. Surfactants Deterg.*, 13 (2010) 247.
19. J. Zhang, J. Liu, W. Yu, Y. Yan, L. You and L. Liu, *Corros. Sci.*, 52 (2010) 2059.
20. J. Cruz, R. Martínez, J. Genesca and E. García-Ochoa, *J. Electroanal. Chem.*, 566 (2004) 111.
21. S.L. Wu, Z.D. Cui, F. He, Z.Q. Bai, S.L. Zhu and X.J. Yang, *Mater. Lett.*, 58 (2004) 1076.
22. J.O'M. Bockris and D. Drazic, *Electrochim. Acta*, 7 (1962) 293.
23. D.A. López, T. Pérez and S.N. Simison, *Mater. Des.*, 24 (2003) 561.
24. H.M. Ezuber, *Mater. Des.*, 30 (2009) 3420.
25. Q. Qu, J. Ma, L. Wang, L. Li, W. Bai and Z. Ding, *Corros. Sci.*, 53 (2011) 1186.
26. X. Liu, Y. G. Zheng and P. C. Okafor, *Mater. Corros.*, 60 (2009) 507.
27. J.A. Mollica, G.R. Padmanabhan and R. Strusz, *Anal. Chem.*, 45 (1973) 1859.
28. J. Porcayo-Calderon, M. Casales-Diaz, L.M. Rivera-Grau, D.M. Ortega-Toledo, J.A. Ascencio-Gutierrez and L. Martinez-Gomez, *J. Chem.*, 2014 (2014) 1.
29. M.A. Amin, M.A. Ahmed, H.A. Arida, F. Kandemirli, M. Saracoglu, T. Arslan and M.A. Basaran, *Corros. Sci.*, 53 (2011) 1895.
30. H. Ma, S. Chen, B. Yin, S. Zhao and X. Liu, *Corros. Sci.*, 45 (2003) 867.
31. P. Bommersbach, C. Alemany-Dumont, J.P. Millet and B. Normand, *Electrochim. Acta*, 51 (2005) 1076.
32. D. Wang, S. Li, Y. Ying, M. Wang, H. Xiao and Z. Chen, *Corros. Sci.*, 41 (1999) 1911.
33. D. Bajpai and V.K. Tyagi, *J. Oleo Sci.*, 55 (2006) 319.

© 2018 The Authors. Published by ESG (www.electrochemsci.org). This article is an open access article distributed under the terms and conditions of the Creative Commons Attribution license (<http://creativecommons.org/licenses/by/4.0/>).